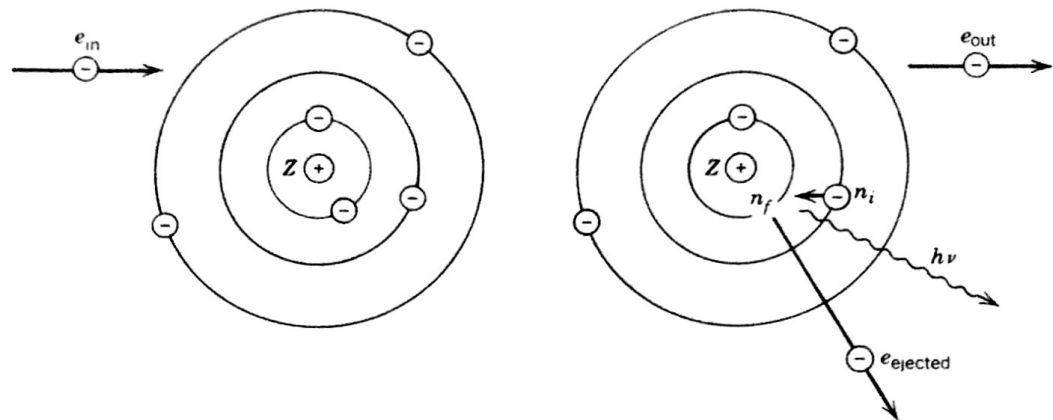


Figure 3-19

Orbital model of atomic excitation and x-ray emission. The collision of a beam electron with a target atom causes an atomic electron to be ejected from an inner orbit. Another atomic electron fills the vacancy and emits an x-ray photon. The deexcitation of the atom occurs between Bohr orbits labeled by the quantum numbers n_i and n_f .



The discrete lines are attributed in either case to transitions between the quantized energy levels of the corresponding atom. X-ray spectral lines have short wavelengths of nanometer order, and so x-ray transition energies of the atom are in the keV range. The large energy required to excite the atom is supplied by the electron beam in the high-voltage tube.

X-ray spectra are associated with complex atoms containing many electrons. This apparent complication is not a serious analytical problem in the x-ray regime because the excitation energies are large enough to remove a tightly bound electron from an *inner* orbit near the nucleus of the atom. In this circumstance the emitted x rays are assumed to result from the transitions of a *single* electron while the other electrons are regarded as spectators. Bohr's simple one-electron model is quite useful in such a situation.

Let us visualize the x-ray excitation and emission processes in the many-electron atom in terms of a system of independent electrons occupying a collection of quantized Bohr orbits. We label the orbits allowed for an individual electron by the familiar quantum number n , in the manner of Equations (3-50) and (3-52). The electrons of interest for the excitation process are those in the innermost orbits of the atom, the so-called *K* and *L* orbits, where the quantum numbers are given by $n = 1$ and $n = 2$. Figure 3-19 shows a model of such a system in which the atomic electrons are distributed over several different Bohr orbits. The figure also shows how the atom becomes excited when the system is struck by an energetic incident electron, as in the bombardment of the target in an x-ray tube. The collision causes the ejection of an atomic electron from an inner orbit, so that the resulting singly ionized atom is left in a highly excited state. The ion deexcites when one of the remaining electrons makes a quantum jump from an outer orbit and fills the vacancy left by the ejected electron. This transition to a state of lower energy is accompanied by the emission of an x-ray photon. The so-called *K* and *L* series of x rays result from all such electron transitions to the $n = 1$ and $n = 2$ inner orbits of the ion.

The first comprehensive study of characteristic x rays was conducted in 1913 by H. G. J. Moseley. He investigated the *K* and *L* spectra of many of the elements in the

periodic table and based his analysis on the notion of inner-electron behavior in the context of Bohr's model. His survey of the elements revealed regularities that finally established the identity between the nuclear charge index Z and the atomic number in the periodic table.

Let us show how the Bohr model is applied in Moseley's analysis. We refer to Figure 3-19 and consider the transition of orbits for a single electron from n_i to n_f , ignoring all the other electrons in the atom. The wavelength of the emitted x ray is given in terms of these quantum numbers by Equation (3-58). Let us rewrite the formula as an expression for the x-ray frequency:

$$\frac{E}{h} = \frac{c}{\lambda} = \nu = Z_{\text{eff}}^2 c R \left(\frac{1}{n_f^2} - \frac{1}{n_i^2} \right). \quad E = Z_{\text{eff}} c h R \left(\frac{1}{n_f^2} - \frac{1}{n_i^2} \right) \quad (3-62)$$

This equation contains an all-purpose Rydberg constant R representing the quantity $\mu R_\infty / m_e$ and an effective charge parameter Z_{eff} replacing the usual nuclear charge index Z . We use Z_{eff} instead of Z because the electron in transition sees a nuclear charge smaller than Ze as the other atomic electrons tend to screen the nucleus from view. Even an inner electron in transition experiences this screening effect to some degree. We can build the effect into the model if we introduce an empirical screening constant (z) and set

$$Z_{\text{eff}} = Z - z_f. \quad (3-63)$$

It is expected that z_f should *increase* with the final quantum number n_f , because the final orbit radius increases with n_f and because the screening is greater for transitions to larger final orbits. Equation (3-63) may be inserted into Equation (3-62), and the result can be rearranged to give the following expression for Z_{eff} :

$$Z - z_f = \frac{\sqrt{\nu}}{\sqrt{cR(1/n_f^2 - 1/n_i^2)}}.$$

This formula becomes

$$Z = z_K + \frac{\sqrt{\nu}}{\sqrt{cR(1 - 1/n_i^2)}} \quad \text{with } n_i = 2, 3, \dots, \quad (3-64)$$

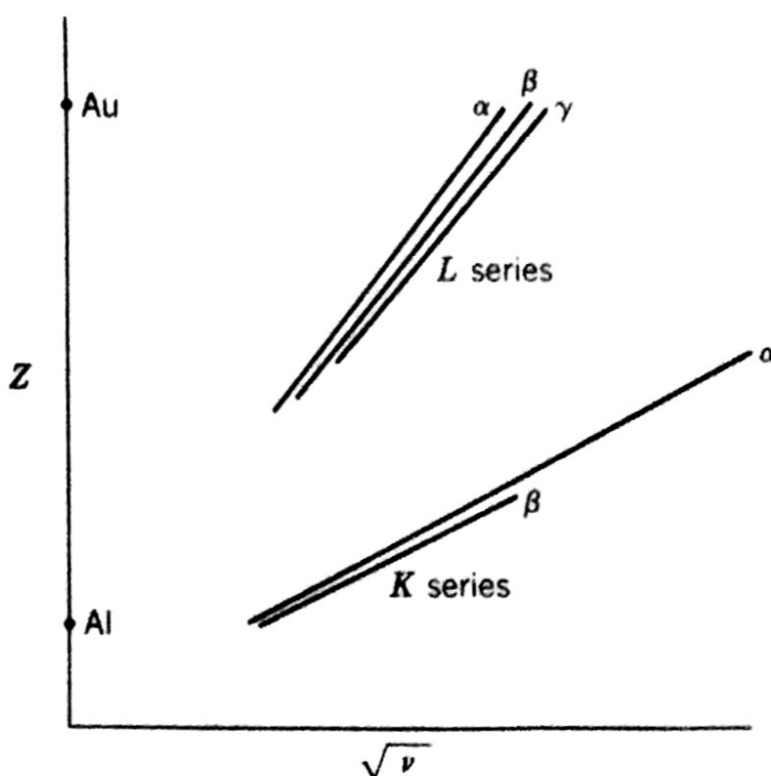
when we choose $n_f = 1$ and consider the K series, and becomes

$$Z = z_L + \frac{\sqrt{\nu}}{\sqrt{cR(1/4 - 1/n_i^2)}} \quad \text{with } n_i = 3, 4, 5, \dots, \quad (3-65)$$

when we choose $n_f = 2$ and consider the L series. The equations predict *linear* relations between Z and $\sqrt{\nu}$, with different intercepts and different sets of slopes in each series. The K series includes K_α and K_β spectral lines for $n_i = 2$ and 3, with corresponding slopes $\sqrt{4/3cR}$ and $\sqrt{9/8cR}$. The L series includes L_α , L_β , and L_γ lines for $n_i = 3, 4$, and 5, with slopes $\sqrt{36/5cR}$, $\sqrt{16/3cR}$, and $\sqrt{100/21cR}$. Figure 3-20 shows sets of Z versus $\sqrt{\nu}$ graphs whose linear behavior reflects these predictions of the one-electron model.

Figure 3-20

Graphs of the atomic number versus the square root of the x-ray frequency in Moseley's analysis.



Moseley was able to change targets in his x-ray tube and observe the frequencies of x rays for more than 40 of the elements between aluminum and gold in the periodic table. He treated Z as the atomic number for each of the elements in the table and plotted his observations in the manner of Figure 3-20. The linear relations between Z and $\sqrt{\nu}$ were confirmed, and the slopes were found to agree with expectations from the Bohr model for the K_α and L_α lines. Approximate values were also deduced for the intercepts of the straight lines in the two series:

$$z_K = 1 \quad \text{and} \quad z_L = 7.4.$$

Moseley's procedures resolved certain questionable assignments of elements in the periodic table and eventually superseded existing chemical methods for identifying new elements. The most important result of his work was the conclusive demonstration that the atomic number, the nuclear charge index, and the number of electrons in the neutral atom were all given by the same quantity Z .

Figure 3-19 can be used to describe two other related phenomena. Both of these possible processes involve the ejection of *two* atomic electrons instead of the one shown in the figure. The primary types of x-ray lines are produced in the transitions of singly ionized atoms, as discussed above. Doubly ionized atoms can also be formed when electrons collide with atoms in the target of an x-ray tube. The orbit structure in the resulting ion is somewhat different from the singly ionized case, and so the radiative transitions in this system produce x rays with correspondingly different frequencies. These x rays appear in the spectrum as secondary satellites to the primary spectral lines. The ejection of a second electron can also occur in an entirely different *radiationless* process, first observed by P. Auger in 1925. The phenomenon, known as the *Auger effect*, is initiated by the excitation of the atom to a singly ionized configuration containing the usual sort of inner-electron vacancy. The ion does not deexcite by photon emission, however; instead, the system spontaneously ejects another electron and becomes a doubly ionized atom. In such a process the second

electron carries away kinetic energy

$$K = E_i^{(1)} - E_f^{(2)},$$

where the notation for the initial and final energies refers to the singly and doubly ionized configurations. Thus, the system in the figure releases energy in the transition $n_i \rightarrow n_f$, and the transition energy is immediately absorbed through an *internal conversion* mechanism in which the second electron is detached and *no* radiation is produced. The emission of an Auger electron is also called *autoionization*; this effect is generally observed in competition with the emission of an x ray.

Example

Moseley's x-ray spectrum of zinc includes the wavelength $\lambda = 0.1445$ nm. We can analyze this particular line by choosing $n_i = 2$ in Equation (3-64) to get

$$\begin{aligned} Z - z_K &= \sqrt{\frac{\nu}{(3/4)cR}} = \sqrt{\frac{4}{3\lambda R}} \quad \leftarrow \quad \lambda = \frac{c}{\nu} \\ &= \sqrt{\frac{4}{3(1.445 \times 10^{-10} \text{ m})(1.097 \times 10^7 \text{ m}^{-1})}} = 29.00. \end{aligned}$$

The intercept for the *K* series is given empirically as $z_K = 1$. Hence, our calculation tells us that Z should be equal to 30, in excellent agreement with the known atomic number of Zn.

3-8 Atomic Processes and the Excitation of Atoms

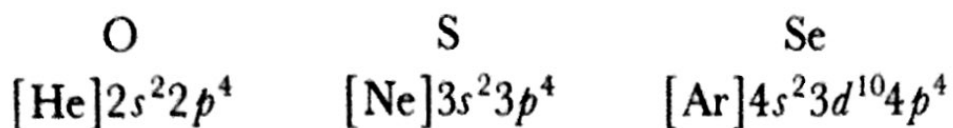
Every atomic system is represented in Bohr's theory by a set of stationary quantized energy states. The theory requires all atoms of a given element to have the same ground state and the same excited states, and so the basic observable properties of the element must somehow reflect the energy level structure of the corresponding atom. All sorts of atomic processes can be examined experimentally to deduce various aspects of this structure.

The atom has been presented as a system of electron orbits in Figure 3-19. We should regard the orbital picture as a primitive quasiclassical device and turn instead to Bohr's discrete energy states for a proper quantum view of the atom. Let us visualize the atomic processes in terms of this new language and look at some of the different forms of interaction between the atom and radiation. Figure 3-21 illustrates several of these phenomena, where each is initiated by an incident photon of energy $h\nu$. We represent the atom by the associated set of energy levels, and we assume the effect of atomic recoil to be negligible in each case.

Elastic photon scattering appears in part (a) of the figure. The atom remains in its ground state as shown, so that the incoming and outgoing photons have the same energy $h\nu$. No other form of interaction can occur if the wavelength of the incident radiation is large compared to the size of the atom. The process is given the name *Rayleigh scattering* in this circumstance because the results are adequately described by Rayleigh's classical scattering theory for electromagnetic waves.

Example

Oxygen, sulfur, and selenium occur in the same column of the periodic table at $Z = 8, 16$, and 34 . The ground-state configurations describe an unfilled p subshell with two electron vacancies in each case:



These elements can fill their vacancies by accepting electrons from two hydrogen atoms to form the molecules H_2O , H_2S , and H_2Se . The two vacant sites in O, S, and Se have angular probability distributions characteristic of an $\ell = 1$ subshell. We can interpret the three m_ℓ assignments for $\ell = 1$ in terms of large distributions of probability along three perpendicular directions. Therefore, we expect to find right-angle shapes when we attach two H atoms to O, S, and Se to make the three triatomic molecules. This expectation is borne out since the hydrogen bonds are at angles of 105° , 93° , and 90° in H_2O , H_2S , and H_2Se . (The angle tends to exceed 90° because of Coulomb repulsion between the two hydrogens and approaches 90° in the largest molecule where the repulsion is weakest.)

9-4 X-Ray Spectra

The periodic table organizes the states of electrons outside closed subshells as the basis for the low-energy regularities of atoms. The underlying shell theory also governs the *inner* shells of the atom where the electrons engage in higher-energy processes such as the emission of x rays. This inner-shell behavior can be examined in a given atom by analyzing an x-ray spectrum like the one shown in Figure 9-8. We have discussed the production of x rays in Section 2-6, and we have taken a preliminary look at characteristic x rays as a source of inner-electron information in Section 3-7. We now return to the study of x-ray spectra with a proper quantum theory at our disposal and find that the independent-electron model provides an especially suitable approach.

Let us reconsider our previous picture of x-ray emission in Figure 9-3 and visualize the excitation and deexcitation of the system from the viewpoint presented in Figure 9-9. The revised picture describes these processes in terms of the single-electron energy levels in the central-field model. We represent the collisional excitation of the atom by the creation of a vacancy, or *hole*, in one of the fully occupied inner subshells. The

Figure 9-8

X-ray lines in the K and L series of tungsten. The heights of the lines are indicative of the observed intensities. The $K\alpha_1$ line at 0.0209100 nm is used to define an x-ray wavelength standard.

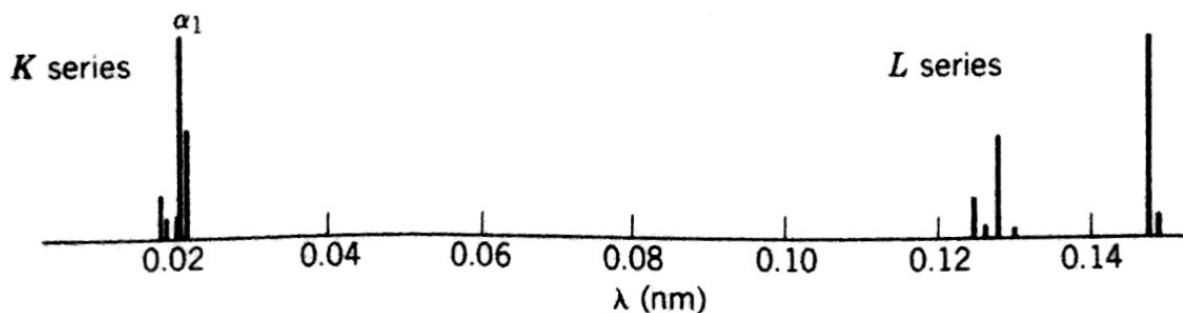
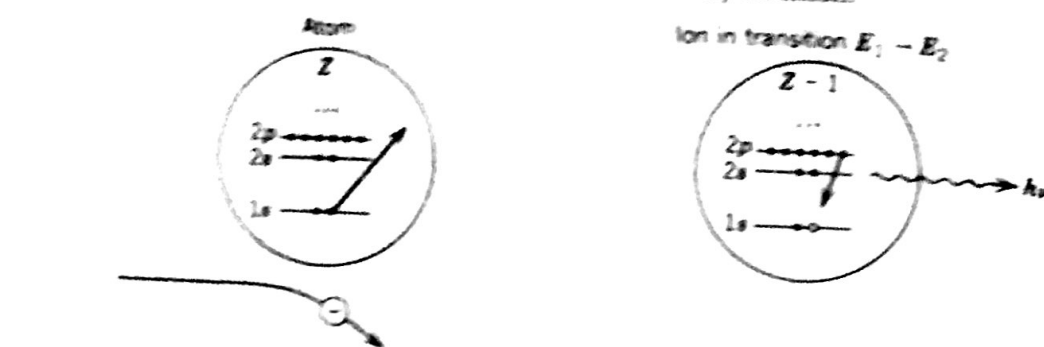


Figure 9-4

Excitation and deexcitation processes associated with x-ray emission.



result is the formation of a highly excited ionic state with initial energy E_1 . We then represent the radiative deexcitation of the system by letting an electron from a higher subshell fill the hole and emit an x-ray photon. The emitted photon has energy

$$h\nu = E_1 - E_2, \quad (9-11)$$

where E_2 is the energy of the excited final state in which the vacancy appears in the higher subshell. Observe from the figure that the x-ray transition occurs in the ion containing $Z - 1$ electrons. Note especially that a vacancy in a higher-energy subshell corresponds to a lower energy state of the ion, so that a hole stands for an absence of energy, as well as charge, in the overall electron system.

Let us also consider the related quantum phenomenon of x-ray absorption. This process is an example of the familiar photoelectric effect, where the absorption of an x-ray photon excites the atom above its ionization level and ejects a bound electron. A quantum mechanical probability can be introduced to describe the photon-atom interaction, and an absorption cross section can be defined to account for the behavior of a beam of x rays incident on the atoms in a sample of matter. We measure absorption in the laboratory by observing the attenuation of an x-ray beam in its passage through a thickness of material. The fractional decrease in intensity $-dI/I$ is related to the element of thickness dx by the proportionality

$$-\frac{dI}{I} = \mu_x dx,$$

where the constant μ_x defines the absorption coefficient of the material. This expression is easily integrated to give the intensity as a function of distance x through the sample, starting with incident intensity I_0 :

$$\int_{I_0}^I \frac{dI}{I} = - \int_0^x \mu_x dx \Rightarrow \ln \frac{I}{I_0} = -\mu_x x \Rightarrow I = I_0 e^{-\mu_x x}.$$

The absorption coefficient varies with the material and depends on the wavelength of the x rays. We can use measurements of the attenuation to determine this dependence, and we can then infer the related behavior of the absorption cross section for the given element.

Figure 9-10

K and *L* absorption edges of lead. The wavelength thresholds occur where the x-ray photon energy becomes insufficient to eject a *K*- or *L*-shell electron. Emission lines of lead in the *K* and *L* series are also shown.

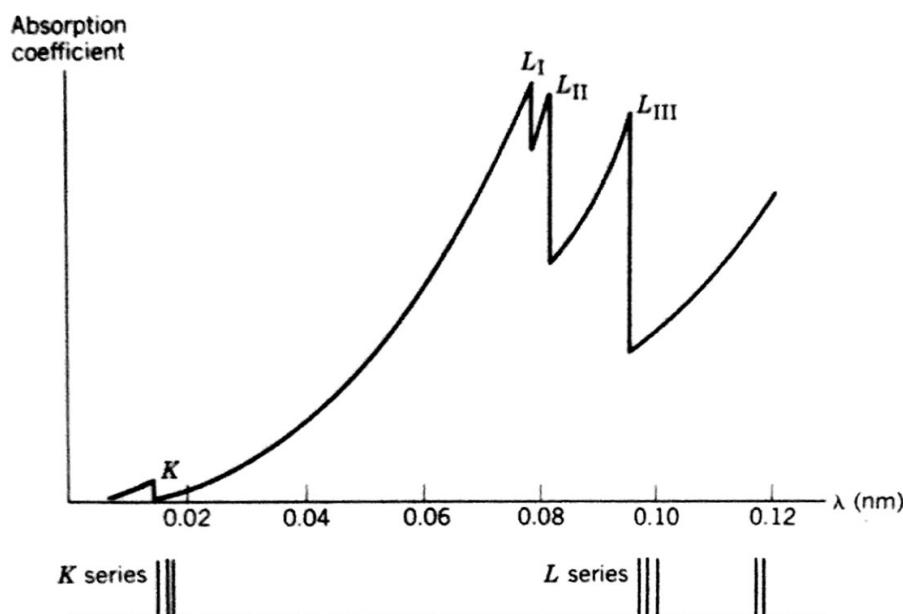


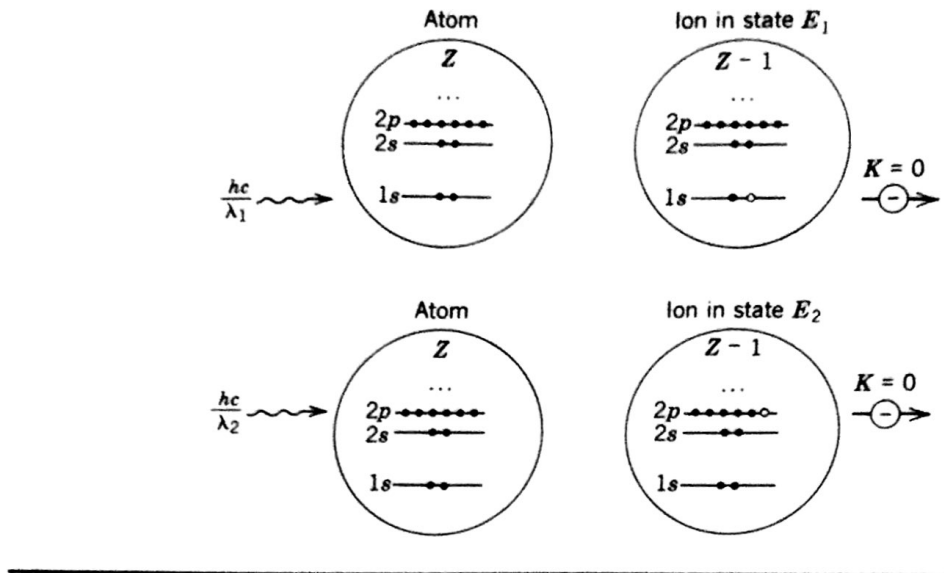
Figure 9-10 shows a typical graph of μ_x as a function of the wavelength λ . We observe zero absorption in the limit $\lambda \rightarrow 0$. This observation tells us that the absorbing medium is transparent to x rays when the beam energy is very large. We then observe a steady growth in absorption as the photon energy decreases from large values and as λ increases from zero, until we reach a sharp value of λ where the medium suddenly becomes transparent again. This feature of the graph is called an *absorption edge*, the first of several to appear with increasing λ in the figure. The indicated *K* absorption edge occurs at wavelength λ_K , where the photon energy is the minimum needed to ionize the atom and leave a vacancy in the *K* shell. When λ becomes larger than λ_K , the x-ray photon energy becomes too small to free a *K*-shell electron but remains large enough to eject an electron from an *L* (or higher) shell. We again observe a steady growth in absorption as the wavelength continues to increase until we reach one of the indicated *L* absorption edges. The various absorption thresholds are tabulated along with the characteristic x-ray emission lines. Both features provide a signature of the particular atom, and both give an indication of the energy levels of the system. We include the emission lines of the *K* and *L* series in the figure so that we can note the positions of these spectral lines relative to the absorption edges.

X-ray absorption can be interpreted with the aid of our representation of the atom as a collection of occupied subshells. Figure 9-11 describes the process in these terms at two different wavelength thresholds. The wavelengths λ_1 and λ_2 correspond to photons whose energies just suffice to eject an electron with no kinetic energy from the particular subshells shown in the figure. We leave the excited ion in states of energy E_1 and E_2 in the two cases, and we note the relation

$$E_1 > E_2 \quad \text{for} \quad \lambda_1 < \lambda_2.$$

Figure 9-11

X-ray absorption processes at two different absorption edges.



The figure tells us that the wavelengths and energies obey the formulas

$$\frac{hc}{\lambda_1} = E_1 - E_{\text{atom}} \quad \text{and} \quad \frac{hc}{\lambda_2} = E_2 - E_{\text{atom}}, \quad (9-12)$$

where E_{atom} denotes the energy of the initial atom. If we compare Figures 9-9 and 9-11, we see that the two ionic energies are the same as the energies E_1 and E_2 in Equation (9-11). If we combine Equations (9-11) and (9-12), we establish the following connection between x-ray absorption and x-ray emission:

$$h\nu = \frac{hc}{\lambda_1} - \frac{hc}{\lambda_2}. \quad (9-13)$$

This formula relates the wavelengths for two absorption edges to the frequency for a certain emission line in the spectrum of a given element. The equality implies an inequality of the form

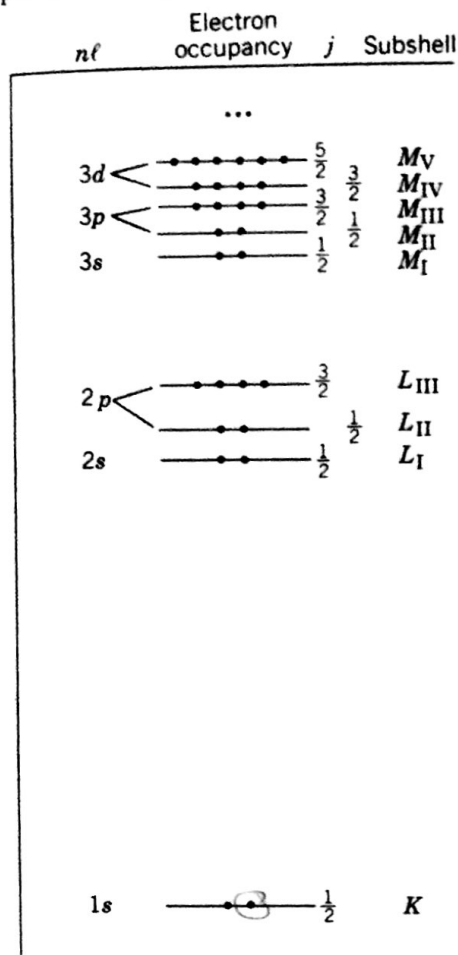
$$\frac{hc}{\lambda} < \frac{hc}{\lambda_1} \quad \text{or} \quad \lambda > \lambda_1$$

for an emitted x ray of wavelength $\lambda = c/\nu$. This observation explains why the lines in a given series have wavelengths *above* the corresponding absorption edge, as indicated in Figure 9-10.

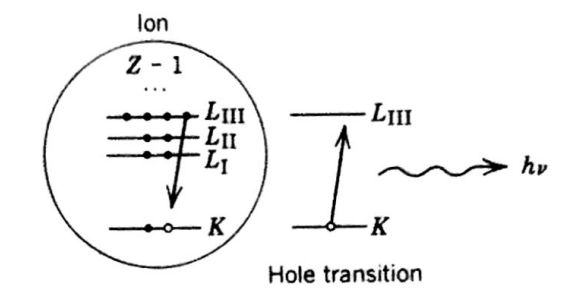
The absorption and emission of x rays reveal a new problem that requires an amendment to the central-field model. Figure 9-10 shows the existence of *three L* absorption edges instead of the two expected for the $2s$ and $2p$ subshells in the *L* shell. This behavior is a clear indication that the $n\ell$ assignments of the model are not adequate to describe the energy levels of the independent electrons. The effect is reminiscent of the multiplet structure of the one-electron atom and is attributable to a

Figure 9-12

Single-electron subshells including the effect of spin-orbit coupling.

**Figure 9-13**

X-ray emission associated with the transition $K \rightarrow L_{\text{III}}$. An electron in the L_{III} subshell fills a vacancy in the K shell while the hole makes a transition from K to L_{III} . The standard $K\alpha_1$ line of tungsten corresponds to this transition.



spin-orbit coupling experienced by each electron in addition to its interaction with the central field. We discuss some of the details of this coupling at the end of the section.

Figure 9-12 shows how these considerations alter the independent-electron picture of the atom by the introduction of the quantum number j . We let each energy level with subshell quantum numbers n and ℓ be *split* for $\ell \neq 0$ in the manner of Figure 8-28, and we recall the familiar quantum numbers $(n\ell jm_j)$ to specify the new single-electron states. We also label the energy levels by the *x-ray spectroscopic notation*

$$K \quad L_1 \quad L_{\text{II}} \quad L_{\text{III}} \quad M_1 \quad M_{\text{II}} \quad M_{\text{III}} \quad M_{\text{IV}} \quad M_{\text{V}} \quad \dots$$

according to the tabulation given in the figure. The exclusion principle is built into this new scheme of states by stipulating that no two electrons are allowed to have the same four quantum numbers $(n\ell jm_j)$. Hence, each of the split $n\ell j$ subshells has a maximum occupancy equal to $2j + 1$, corresponding to the number of degenerate m_j states for the given value of j . (We note in passing that the figure orders the energies of the inner subshells in ascending fashion as

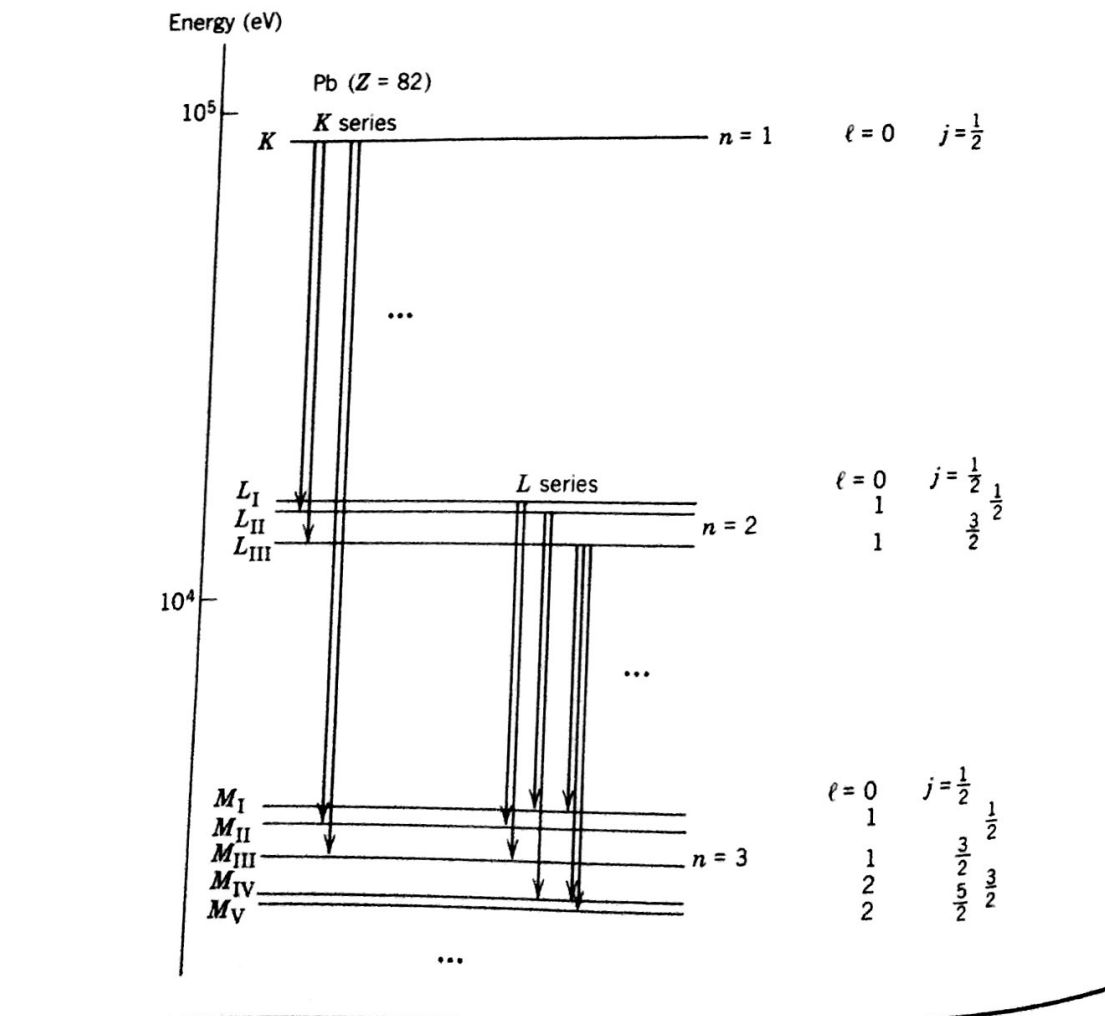
$$1s \quad 2s \quad 2p \quad 3s \quad 2p \quad 3d \quad \dots$$

This ordering of values of E_{nl} holds for the inner electrons of a large- Z atom.) We note especially that the occurrence of the three split L subshells in Figure 9-12 is directly correlated with the existence of the three L absorption edges in Figure 9-10.

Let us now return to our picture of x-ray emission in Figure 9-9 and revise the diagrams to account for the splitting of the subshells. We illustrate the result in Figure 9-13 in terms of a particular x-ray transition. The indicated process shows the filling of an inner-shell hole by an electron from a higher subshell, along with the corresponding transition of the hole in the *opposite* direction. Since the initial and final states of the ion are associated with the location of the hole, it is conventional to represent the process as a *hole transition*. The convention employs an energy level diagram in which the highest energy state refers to a hole in the K shell, and in which the zero level refers to the ionic ground state where the hole occurs just beyond all the electron subshells. This presentation of the energy states of the ion *inverts* our view of the levels found in Figure 9-12 and produces an *x-ray level diagram* of the kind shown in Figure 9-14. The figure lists the values of the hole quantum numbers ($n\ell j$) and indicates the allowed hole transitions. These radiative processes are governed by the electric dipole selection rules, so that the single-particle quantum numbers are

Figure 9-14

X-ray levels of lead and transitions allowed by the electric dipole selection rules. The energies are plotted on a logarithmic scale.



supposed to change according to the conditions

$$\Delta\ell = \pm 1 \quad \text{and} \quad \Delta j = 0 \text{ or } \pm 1 \quad (\text{but } 0 \not\rightarrow 0),$$

as in Equations (8-42) and (8-43). The various transitions are organized in the diagram into the different series of emission lines. We can employ this same general scheme whenever we wish to analyze the x-ray spectrum of any element.

Detail

We can formulate the spin-orbit interaction for an electron in a complex atom by constructing a parallel with the expression for the one-electron atom. Let us return to Equation (8-32) and rewrite the expression in terms of a derivative of the Coulomb potential energy:

$$V_{SL} = \frac{\mathbf{S} \cdot \mathbf{L}}{2m_e^2 c^2} \frac{1}{r} \frac{dV}{dr},$$

where

$$V = -\frac{Ze^2}{4\pi\epsilon_0 r} \quad \text{and} \quad \frac{1}{r} \frac{dV}{dr} = \frac{Ze^2}{4\pi\epsilon_0 r^3}.$$

An electron in the central-field model has central potential energy $V_c(r)$, and so the spin-orbit interaction of the electron in the complex atom must have the form

$$V_{SL} = \mathbf{S} \cdot \mathbf{L} \xi_c(r)$$

in which

$$\xi_c(r) = \frac{1}{2m_e^2 c^2} \frac{1}{r} \frac{dV_c}{dr}.$$

The function $V_c(r)$ contains the nuclear screening factor $Z_{\text{eff}}(r)$. This quantity varies between the value Z at small r and the value unity at large r , so that spin-orbit coupling becomes stronger with increasing Z , especially in states where r has a small average value. We know from Section 8-9 how the interaction V_{SL} perturbs the energy states in a central field. Let us consider an independent electron in an $n\ell$ subshell and describe the electron states by means of the quantum numbers $(n\ell jm_j)$ instead of the spin-orbital set $(n\ell m_\ell m_s)$. We use the eigenfunction $\psi_{n\ell jm_j}$ as before to calculate the expectation value of V_{SL} , and we obtain the following results:

$$\begin{aligned} \langle V_{SL} \rangle &= \left\langle \frac{J^2 - L^2 - S^2}{2} \xi_c(r) \right\rangle \\ &= \frac{\hbar^2}{2} \left[j(j+1) - \ell(\ell+1) - \frac{3}{4} \right] \langle \xi_c(r) \rangle \\ &= \frac{\hbar^2}{2} \langle \xi_c(r) \rangle \cdot \begin{cases} \ell & \text{for } j = \ell + \frac{1}{2} \\ -\ell - 1 & \text{for } j = -\ell - \frac{1}{2}. \end{cases} \end{aligned}$$

This energy shift affects the energy level of an electron in an $n\ell$ subshell according to the value of j and causes a splitting in every subshell with $\ell \neq 0$.

Example

The K and L_{III} absorption edges of lead in Figure 9-10 are observed at 0.01408 and 0.09511 nm. Let us consult Equation (9-13) and use these numbers to compute the wavelength emitted in the $K \rightarrow L_{\text{III}}$ transition:

$$\frac{1}{\lambda(KL_{\text{III}})} = \frac{1}{\lambda_K} - \frac{1}{\lambda_{L_{\text{III}}}} = \frac{1}{0.01408 \text{ nm}} - \frac{1}{0.09511 \text{ nm}} = \frac{1}{0.01653 \text{ nm}}.$$

This emission line can also be predicted from the energies of the K and L_{III} x-ray levels of lead. We use the tabulated values $E_K = 88.00 \text{ keV}$ and $E_{L_{\text{III}}} = 13.03 \text{ keV}$, and we find

$$\lambda(KL_{\text{III}}) = \frac{hc}{E_K - E_{L_{\text{III}}}} = \frac{1.240 \text{ keV} \cdot \text{nm}}{74.97 \text{ keV}} = 0.01654 \text{ nm}.$$

Both calculations agree with the wavelength listed in the tables for the KL_{III} line of lead. The line and the transition are included among the information given in Figures 9-10 and 9-14.

9-5 Electron Antisymmetry

We have been able to implement the exclusion principle and explain the periodic table with only minimal use of quantum mechanics. The exclusion principle itself has been expressed in a limited context, based entirely on the assignment of electron quantum numbers in the central-field model. We now want to examine the fundamental quantum nature of Pauli's principle from the viewpoint of *electron indistinguishability* and develop the broader concept of *identical-particle symmetry*. We recall that we have already introduced this notion in the framework of one-dimensional quantum mechanics in Section 5-10.

Let us begin with the two-electron system and identify the degrees of freedom to be the pair of spatial coordinates and spin orientations

$$(\mathbf{r}_1, S_{1z}) \quad \text{and} \quad (\mathbf{r}_2, S_{2z}).$$

It is convenient to symbolize these variables in the wave function by adopting the abbreviated notation

$$\Psi(\mathbf{r}_1, S_{1z}, \mathbf{r}_2, S_{2z}, t) = \Psi(1, 2, t).$$

We then determine the probability of finding the two particles in two volume elements $d\tau_1$ and $d\tau_2$ at time t by evaluating the expression

$$|\Psi(1, 2, t)|^2 d\tau_1 d\tau_2.$$

The electrons in the system have identical physical attributes of charge $-e$, mass m_e , and spin $s = \frac{1}{2}$. It is not meaningful to refer to these particles as electron 1 and electron 2 because the notation implies that the two electrons can always be distinguished in any state. The intrinsic indistinguishability of identical quantum par-